Chapter 4

Impact of cosmic ray protons during cosmic dawn and epoch of reionization*

On what can we now place our hopes of solving the many riddles which still exist as to the origin and composition of cosmic rays?

– Victor Francis Hess

As we discussed in the chapter 2, the decay of the primordial magnetic field prevents it to be a significant source of heating during cosmic dawn, in this chapter, we explore another possible source of IGM heating, namely, the cosmic rays generated from the first

*This chapter is adapted from the paper, "Impact of cosmic rays on the global 21-cm signal during cosmic dawn" by Bera, Samui, and Datta (2023).

generation of galaxies. The possibilities of heating and ionization of the IGM by cosmic rays from young galaxies are already discussed by Ginzburg and Ozernoi (1966); Nath and Biermann (1993); Samui, Subramanian, and Srianand (2005); Samui, Subramanian, and Srianand (2018) in the context of reionization and post-reionization era. Further, the impact of cosmic rays generated from microquasars on the reionization was discussed in Tueros, del Valle, and Romero (2014). However, there has been only a handful of earlier works that discuss the effect of cosmic ray heating during the cosmic dawn and its consequences on the global 21-cm signal (Sazonov and Sunyaev, 2015; Leite et al., 2017; Jana, Nath, and Biermann, 2019). Among them, Sazonov and Sunyaev (2015) has adopted a simplified approach by assuming that a small fraction of supernovae kinetic energy goes into the IGM heating without any detailed modeling of the energy transfer. They did not consider contributions from Pop III and Pop II stars separately as well. Moreover, the effects of cosmic rays coming from early epochs are also not considered by Sazonov and Sunyaev (2015) as well as in Jana, Nath, and Biermann (2019). On the other hand, Leite et al. (2017) modeled the propagation of cosmic rays in the IGM but neither considered the detailed model of the star formation in Pop III and Pop II galaxies nor the 21-cm signal.

Here we investigate, in more detail, the heating of the IGM by cosmic rays from Pop II and Pop III stars and their impact on the global HI 21-cm signal during cosmic dawn. We model the contributions of cosmic rays from Pop III stars and Pop II stars separately as they are expected to produce different supernovae. Further, we consider more detailed modeling of star formation by taking into account various feedbacks like Lyman-Warner feedback, supernova, radiative feedback, etc., discussed in the previous chapter. Moreover, our model accounts for the evolution/propagation of cosmic ray particles from previous redshifts, and the energy deposition by these particles are computed in detail instead of adopting a simplified approach as followed in previous studies. Our study also focuses on the standard IGM scenario along with a scenario where dark matter-baryon interaction is considered in light of recent observations of the global 21-cm signal. Dark matter-baryon interaction makes the IGM colder as compared to the IGM in the standard

scenario as discussed in sec. 2.2 and we refer to this as the 'cold IGM' scenario. Finally, we show that our cosmic ray heating model can explain the EDGES observations with a reasonable choice of model parameter and thus establishing the importance of detailed modeling of cosmic ray heating. The main purpose of this work is to investigate cosmic rays from Pop III and Pop II stars as a potential source of IGM heating during cosmic dawn. In addition, we present a comparison of the efficiency of cosmic rays heating with the more conventional IGM heating mechanism by X-rays during cosmic dawn.

The structure of this chapter is as follows. In Section 4.1, we outline the evolution of cosmic rays and the energy deposition by these particles into the IGM. We present our results of the spin temperature, T_s, the kinetic temperature, T_g, and finally, the differential brightness temperature, T_{21} highlighting the effect of cosmic ray heating in Section 4.2. This section also highlights the changes in differential temperature due to the variation in assumed model parameters. Finally in Section 4.3, we present our conclusions including the summary of our results.

4.1 Evolution of cosmic rays

Cosmic rays are generated in the termination shock of the supernova explosions originating from both Pop III and Pop II stars. A significant fraction, $\epsilon \sim 0.15$ of the SNe kinetic energy ($E_{\rm SN}$) gets injected into the cosmic rays (Hillas, 2005; Caprioli and Spitkovsky, 2014). Thus the average rate of energy injection per unit physical volume into the cosmic rays (in units of $\rm erg\,s^{-1}cm^{-3}$) can be calculated as (Samui, Subramanian, and Srianand, 2005),

$$\dot{E}_{\rm CR}(z) = 10^{-30}\epsilon \left(\frac{E_{\rm SN}}{10^{51}\,\rm erg}\right) f_{\rm SN} \left(\frac{\rm SFRD(z)}{\rm M_\odot\,yr^{-1}\,Mpc^{-3}}\right)(1+z)^3. \tag{4.1}$$

Here the SFRD(z) is obtained from Eq. 3.2 for Pop III and Pop II stars. Further, $f_{\rm SN}$ is the number of SNe explosions per unit solar mass of star formation. As already mentioned in the chapter 3, we assume a single star of 145 $M_\odot$ is formed in minihalos and explodes as a supernova having energy 10^{52} erg (mid mass range of Mebane, Mirocha, and Furlanetto, 2018). Thus in our model, $f^{\rm SN} \approx 1/145$ and $E_{\rm SN} \sim 10^{52}$ erg for Pop III stars. In case of Pop II stars, we assume that a supernova of energy $E_{\rm SN} \sim 10^{51}$ erg is formed per 50 $M_\odot$ of a star having $1-100$ $M_\odot$ of Salpeter IMF and hence, $f_{\rm SN} = 0.02$ (Samui, Subramanian, and Srianand, 2005).

We note that the cosmic ray protons mostly contribute to the heating of the IGM. In the case of a supernova exploding in minihalos, low energy protons ($\leq$30 MeV) can escape the halo and heat the intergalactic medium via collision with free e^-, and ionization of neutral hydrogen. These SNe are more energetic compared to the core-collapse SNe, and the shock front reaches the virial radius within the Sedov-Taylor (ST) phase itself. Thus the cosmic rays are generated outside the virial radius and get injected into the IGM easily (Sazonov and Sunyaev, 2015). This is contrary to massive atomic cooling halos hosting Pop II stars where the low energy protons get confined within the halo and only high energy protons can escape into the IGM and contribute to the heating (Samui, Subramanian, and Srianand, 2005).

In general, the cosmic ray proton spectra can be modeled as a power law in the

momentum space (Schlickeiser, 2002) which is given by,

$$\frac{dn_{\rm CR}(p,z)}{dt}dp = \dot{N}_0(z)\left(\frac{p}{p_0}\right)^{-q}dp, \tag{4.2}$$

where $\dot{N}_0(z)$ (along with p_0) is the normalization factor which is determined from the total available energies of cosmic rays. It is calculated by integrating $E(p)\dot{N}_0(p/p_0)^{-q}dp$ with a low energy cut-off of 10 keV and equating to $\dot{E}_{\rm CR}(z)$ (Eq. 4.1). The slope of the spectrum, q has a typical value of 2.2 Schlickeiser, 2002 which matches quite well with observations.

Unlike UV photons, the number density of cosmic ray protons in the IGM at a redshift, z is contributed by the cosmic rays generated at z, and cosmic rays that are injected and evolved from higher redshift, $z_i > z$. Therefore, the physical number density of cosmic rays at a redshift z, having velocity between β and $\beta + d\beta$ is given by,

$$N_{\rm CR}(\beta, z, z_0) = \int_{z_0}^{z} dz_i \frac{dn(z_i, p_i)}{dz_i}\frac{dp_i}{d\beta_i}\frac{d\beta_i}{d\beta}\left(\frac{1+z}{1+z_i}\right)^3. \tag{4.3}$$

Here, z_0 is the initial redshift of cosmic ray injection by the first generation of stars and we have taken it to be $z = 50$. Cosmic ray protons are expected to loose their energy while propagating from redshift z_i to z. The redshift evolution of velocity $v = \beta c$ of cosmic ray particles is governed by three processes, (i) the collision with free e^-, (ii) ionization of neutral hydrogen, and (iii) the adiabatic expansion of the universe, and given by (Schlickeiser, 2002),

$$\begin{aligned}\frac{d\beta}{dz} = \frac{1}{H(z)\,(1+z)}\Bigg[&3.27\times10^{-16}n_e(z)\frac{(1-\beta^2)^{3/2}}{\beta}\frac{\beta^2}{x_m^3+\beta^3}\\ &+1.94\times10^{-16}n_{\rm HI}(z)\frac{(1-\beta^2)^{3/2}}{\beta}\frac{2\beta^2}{(0.01)^3+2\beta^3}\\ &\times\{1+0.0185\log\beta\,\Theta(\beta-0.01)\}\Bigg]+\frac{\beta(1-\beta^2)}{(1+z)}\end{aligned} \tag{4.4}$$

where, $n_e(z)$ and $n_{\rm HI}(z)$ are the electron and neutral hydrogen densities respectively in units of $\rm cm^{-3}$, $x_m = 0.0286(T_g/(2\times10^6\,\rm K))^{1/2}$ and Θ is the Heaviside step function.

We note that in Eq. 4.4 the two terms inside the square brackets are due to the collision with free electron and ionization of neutral hydrogen atoms respectively, both of

which deposit energy to the IGM and contribute to heating. In case of a collision with free electrons, the complete energy loss by a cosmic ray proton becomes the thermal energy of the IGM.

However, when the cosmic ray protons interact with the neutral intergalactic medium, it may result in primary ionization or excitation to a discrete level, and the entire energy of the cosmic ray proton does not get transferred to the free electron. It is shown that the number of primary ion formations is almost proportional to the average loss by collision. In fact, one such ion pair gets formed if the primary loss is about 32 eV (discussed in sec. 5.3.11 in Schlickeiser, 2002). The total energy loss rate is then obtained by multiplying the number density of cosmic rays ($N_{\rm CR}$) with average energy loss and dividing by 32 eV. It is shown that for each ionization process, $\Delta Q \simeq 20$ eV gets deposited as heat (Spitzer Jr and Scott, 1969; Goldsmith and Langer, 1978). This leads to a factor of $5/8$ in the calculation of energy deposition by cosmic rays. Hence, the heating rate of the IGM by cosmic ray particles due to ionization can be written as,

$$\Gamma_{\rm CR}(z, z_0) = \frac{5}{8}\eta_1\eta_2\eta_3 \int \frac{dE(\beta)}{dz} N_{\rm CR}(\beta, z, z_0)\, d\beta, \tag{4.5}$$

where, $\eta_1 = 5/3$ occurs due to the secondary ionization by e^- which produces during ionization by primary cosmic ray particles, $\eta_2 \simeq 1.17$ accounts for the 10% He abundance in the IGM, and $\eta_3 \simeq 1.43$ takes into account the contribution of heavy cosmic ray nuclei and cosmic ray electrons (e^-), positrons (e^+) (Schlickeiser, 2002). These energy depositions due to the cosmic ray particles are incorporated in the temperature evolution of IGM i.e. in Eq. 1.9 and as we will see they can contribute as a major heating source of IGM during the cosmic dawn.

As already mentioned, the low-energy protons that take part in collision and ionization do not escape from the massive atomic cooling Pop II galaxies. Only the high-energy protons can escape and may interact with high redshift IGM. It should be noted that a major part of the cosmic ray energy is carried by the high-energy protons (~ 1 GeV). If a sufficient magnetic field (B) is present in the IGM, these high-energy cosmic ray particles can gyrate along the magnetic field lines and generate Alfvén waves. When these

waves get damped, the energy is transferred to the thermal gas (Kulsrud and Pearce, 1969; Skilling, 1975; Bell, 1978; Kulsrud, 2004). The energy deposition rate via this Alfvén wave generation is $|v_A.\nabla P_c|$, where $v_A = B/\sqrt{4\pi\rho}$ is the Alfvén velocity (ρ is the plasma density) and ∇P_c is the cosmic ray pressure gradient. Thus the time scale ($t_{\rm CR}$) for this process to influence the IGM of temperature T_g can be calculated by

$$t_{\rm CR} = \frac{3nk_BT_g}{2|v_A.\nabla P_c|}. \tag{4.6}$$

This time scale should be compared to the Hubble time (t_H) if it can heat the IGM. Putting some reasonable numbers we find (also see Samui, Subramanian, and Srianand, 2018),

$$\frac{t_{\rm CR}}{t_H} \approx 0.16 \left(\frac{h}{0.7}\right)^4 \left(\frac{\Omega_{\rm m}}{0.3}\right)^{1/2} \left(\frac{1+z}{16}\right)^4 \left(\frac{T_g}{10\,{\rm K}}\right) \left(\frac{0.1\,{\rm nG}}{B_0}\right) \times \left(\frac{5\times10^{-5}\,{\rm eV/cm^3}}{E_{\rm CR}}\right) \left(\frac{L}{0.01\,{\rm Mpc}}\right), \tag{4.7}$$

where, L is the physical distance between galaxies and we have taken $L = 0.01$ Mpc as the average separation of typical galaxies at $z = 15$.

Thus we can see if a primordial magnetic field of present-day value, $B_0 = 0.1$ nG (Minoda, Tashiro, and Takahashi, 2019) is present, and cosmic rays have energy density of $E_{\rm CR} = 5 \times 10^{-5}\,{\rm eV/cm^3}$ (this can easily be seen from Eq. 4.1 using SFRD at $z = 15$), the cosmic rays can dissipate their energy to the IGM within Hubble time to influence the IGM temperature of 10 K at $z \sim 15$. Hence, this magnetosonic transfer of energy due to cosmic rays is an important source of IGM heating. To see its influence we assume a fraction $Q_{\rm CR,II}$ of total cosmic ray energy density is transferred as the thermal energy of the IGM via the Alfvén waves from the high energy protons that escape from Pop II galaxies. It has been shown in Samui, Subramanian, and Srianand (2018) that if only 10-20% of cosmic rays energy can be transferred to the IGM it can significantly alter the thermal history of the IGM in the redshift range 2-4. Thus it is natural to consider the same for the thermal history of the IGM during the cosmic dawn.

In late time, along with the ionizing photons, the cosmic rays from the first generation of galaxies are likely to alter the ionization fraction x_e and it is determined by the

second last term in eq. 1.7 where,

$$I_{\rm CR} = \int N_{\rm CR}(\beta, z, z_0)\sigma_{\rm HI}\beta d\beta. \tag{4.8}$$

Here, $\sigma_{\rm HI} = \frac{1.23\times10^{-20}}{\beta^2}\left(6.20 + \log\frac{\beta^2}{1-\beta^2} - 0.43\beta^2\right)$ (Spitzer and Tomasko, 1968). However, we have checked that the cosmic rays can change the ionization fraction at most 10^{-3} for the supernova kinetic energy we considered here which is similar to Sazonov and Sunyaev (2015). Similar results were also obtained by Samui, Subramanian, and Srianand (2005). Since we are interested in 21-cm signal in the redshift range 10 to 20, the 21-cm signal is mostly governed by the temperature differences between the IGM and the background radio signal rather than the ionization fraction of the hydrogen which is at most 0.1 by redshift $z = 10$ thus only altering the 21-cm signal at most 10% level (Furlanetto, Oh, and Pierpaoli, 2006). One should consider the contribution of UV photons from the first stars in order to model the ionization fraction more accurately that we are not taking into account in this particular work as we are interested in the cosmic dawn.

Here, we would like to mention that cosmic ray electrons from first sources can, in principle, generate radio background through their interactions with the intergalactic magnetic field and alter the global 21-cm signal (Jana, Nath, and Biermann, 2019). However, we expect the resulting synchrotron radiation is expected to be insignificant during cosmic dawn given the current upper limit on the intergalactic magnetic field ($B_0 \lesssim 0.1$ nG) (Minoda, Tashiro, and Takahashi, 2019; Bera, Datta, and Samui, 2020).

4.2 Results and Discussion

In this section, we present our results of the global 21-cm signal highlighting the heating due to cosmic ray protons generated through supernova explosions from very early Pop III and Pop II stars. For better comprehension, we list below the default parameters that we used in our work. The reason for considering such parameter values has already been discussed in the previous section.

Pop III model :

- Each minihalo generates a single Pop III star of $145\ M_\odot$ which explodes as a core-collapse supernovae, so $f_{\rm SN,III} = 1/145$.
- The explosion energy of a Pop III supernova is taken as $E_{\rm SN,III} = 10^{52}$ erg.
- A fraction of SNe kinetic energy, $\epsilon_{\rm III} = 0.06$ gets utilised to accelerate the cosmic rays. This value is chosen in order to match the EDGES deep absorption profile, though it is a free parameter in our model and we show the variation of this parameter in the later section.
- The slope, q of the cosmic ray spectra (Eq. 4.2) generated by the supernova, is taken as 2.2.

Pop II model :

- We consider one supernova explosion per $50\ M_\odot$ of star formation, i.e. $f_{\rm SN,II} = 0.02$
- The typical energy of Pop II supernova is $E_{\rm SN,II} = 10^{51}$ erg.
- The fraction of SNe kinetic energy carried by the cosmic rays is $\epsilon_{\rm II} = 0.15$.
- The amount of cosmic ray energy that gets transferred to the IGM and heats the surrounding gas is $Q_{\rm CR,II} = 0.15$. This value is chosen to explain the sharp rise of the EDGES profile. The variation of this parameter is shown in the Fig. 4.3.

These are the default parameter values adopted from Mebane, Mirocha, and Furlanetto (2018) and Samui (2014) for Pop III and Pop II star formation models respectively, and from Schlickeiser (2002) & Samui, Subramanian, and Srianand (2005) for cosmic rays energy deposition. These parameters are chosen keeping in mind the EDGES observation. We also show results by varying parameters such as $q, \epsilon_{\rm III}, \epsilon_{\rm II}$ and $Q_{\rm CR,II}$. As the impact of $\epsilon_{\rm II}$ and $Q_{\rm CR,II}$ are similar, we don't vary them separately rather we vary only $\epsilon_{\rm II}$, and represent it as $\epsilon_{\rm II}$ and/or $Q_{\rm CR,II}$.

4.2.1 Ly-α coupling and resulting spin temperature

In this section, we discuss the Lyman-α coupling of hydrogen spin temperature and IGM temperature due to the Lyman-α flux resulting from the Pop III and Pop II star formation as discussed in section 3.4.

As soon as the first sources appear, Ly-α photons from these sources help the spin temperature T_s to decouple from the CMBR temperature and start coupling with the gas temperature. This can be seen from Fig. 4.1, where we have plotted the CMBR temperature, spin temperature, and gas temperature starting from the recombination redshift $z = 1010$ without DM-b interaction (top panel) and with DM-b interaction (bottom panel). It is clear from the figure that the decoupling begins at a redshift as early as $z \sim 30$ in our model. The spin temperature, T_s then gradually approaches the IGM kinetic temperature, T_g, and gets fully coupled at redshift $z \approx 17$. Since the Pop II stars dominate the Ly-α photon budget at redshift $z \lesssim 20$, the coupling is mainly determined by this population as shown in the top panel of Fig. 4.1, where we plotted the spin temperatures by blue (Pop II), red (Pop III) and black (Pop II + Pop III) dashed curves. We note that along with the standard adiabatic cooling of the IGM prior to the heating, we also consider dark matter-baryon interaction in our work. The bottom panel of Fig. 4.1 shows result in presence of dark-matter baryon interaction for dark matter mass $m_\chi = 0.1$ GeV and the interaction cross-section $\sigma_{45} = \frac{\sigma_0}{10^{-45}\,\mathrm{m}^2} = 2$. This interaction helps to cool the IGM faster compared to the standard adiabatic cooling, as discussed in sec. 2.2. This scenario is motivated by the EDGES observation that shows a strong absorption profile of -0.5 K that is elaborately discussed in sec. 1.4. Redshifts of the decoupling of T_s from the CMBR temperature and coupling to the IGM kinetic temperature can change to some extent depending on the Ly-α escape fraction into the IGM and redshift evolution of the IGM kinetic temperature. However, as we focus on the impact of cosmic rays on the heating of the IGM here, we defer this discussion to future works.

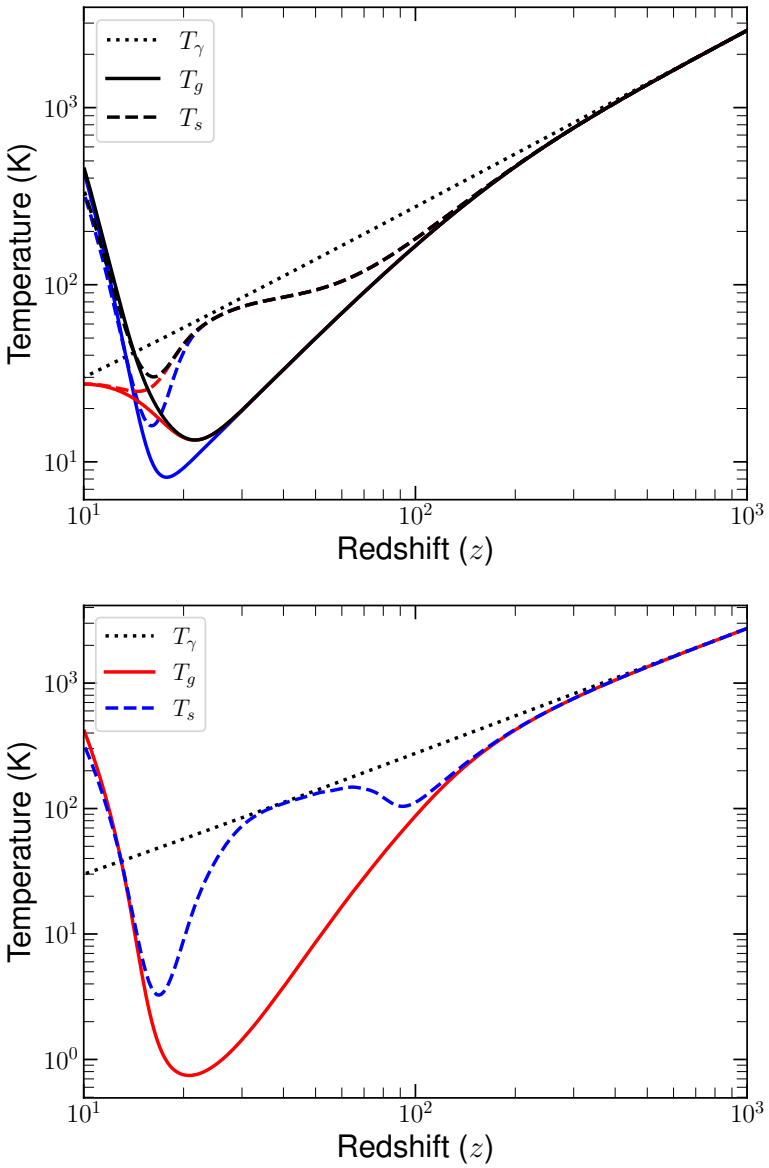

Figure 4.1: **Top panel:** The evolution of the gas kinetic temperature, T_g with redshift is shown by black solid curve along with the spin temperature, T_s, and CMBR temperature T_γ by black dashed and black dotted curves respectively. The blue solid and dashed curves represent the evolution in T_g and T_s respectively for considering the contribution of cosmic rays from Pop II stars only and the red curves represent the same for considering Pop III stars only. **Bottom panel:** The evolution of the gas kinetic temperature, T_g with redshift is shown by red solid curve along with the spin temperature, T_s, and CMBR temperature T_γ by blue dashed and black dotted curves respectively. The dark matter-baryon interaction is included here for excess cooling mechanism keeping in mind the EDGES deep absorption signal. The dark matter mass, and interaction cross-section $(m_\chi/\mathrm{Gev}, \sigma_{45}) = (0.1, 2)$ are considered for this particular plot.

4.2.2 Impact of cosmic rays heating on IGM temperature

One of the major aims of this work is to explore cosmic rays from first generation of stars as a source of IGM heating during the cosmic dawn. This section discusses our results on that. As already discussed, we consider the collisional and ionization interaction as well as the magnetosonic interaction through which the energy gets transferred from cosmic rays to the IGM which leads to the increase in kinetic temperature of the IGM. In Fig. 4.1, we have plotted the resulting IGM gas temperature by the red solid curve. Initially up to redshift $z \gtrsim 200$, the gas kinetic temperature T_g and CMBR temperature T_γ follow each other. This is enabled through the Compton scattering process. Afterward, T_g cools faster than T_γ due to adiabatic cooling and dark matter-baryon interaction that we consider. Fig. 4.1 shows results for the dark matter mass of $m_\chi = 0.1$ GeV, and interaction cross-section of $\sigma_{45} = 2$ that resulted in the sharp fall of IGM temperature. Further, note that, due to the collisional coupling hydrogen spin temperature follows the IGM temperature up to $z \gtrsim 100$. Afterward, the collisional coupling becomes weak due to the lower IGM density and temperature, and hence T_s again starts to follow the CMBR temperature. As discussed before, the spin temperature again decoupled from the CMBR due to the presence of Ly-α photons around $z \sim 30$. Meanwhile, the IGM temperature reaches a minimum at $z \sim 20$. By this time the first generation of stars has produced enough amount of cosmic rays that start heating the surrounding gas and increase the IGM temperature as can be seen from Fig. 4.1. T_g crosses the CMBR temperature at redshift $z \sim 12$ due to the cosmic ray heating. By this redshift, the Ly-α coupling has completely coupled the spin temperature to the gas temperature. The interplay between T_s and T_γ determines the 21-cm brightness temperature that we discuss in the next section.

4.2.3 Global 21-cm signal

The EDGES observation suggests a mean brightness temperature, T_{21} between -0.3 K to -1.0 K. As already discussed, this strong absorption can be explained by considering

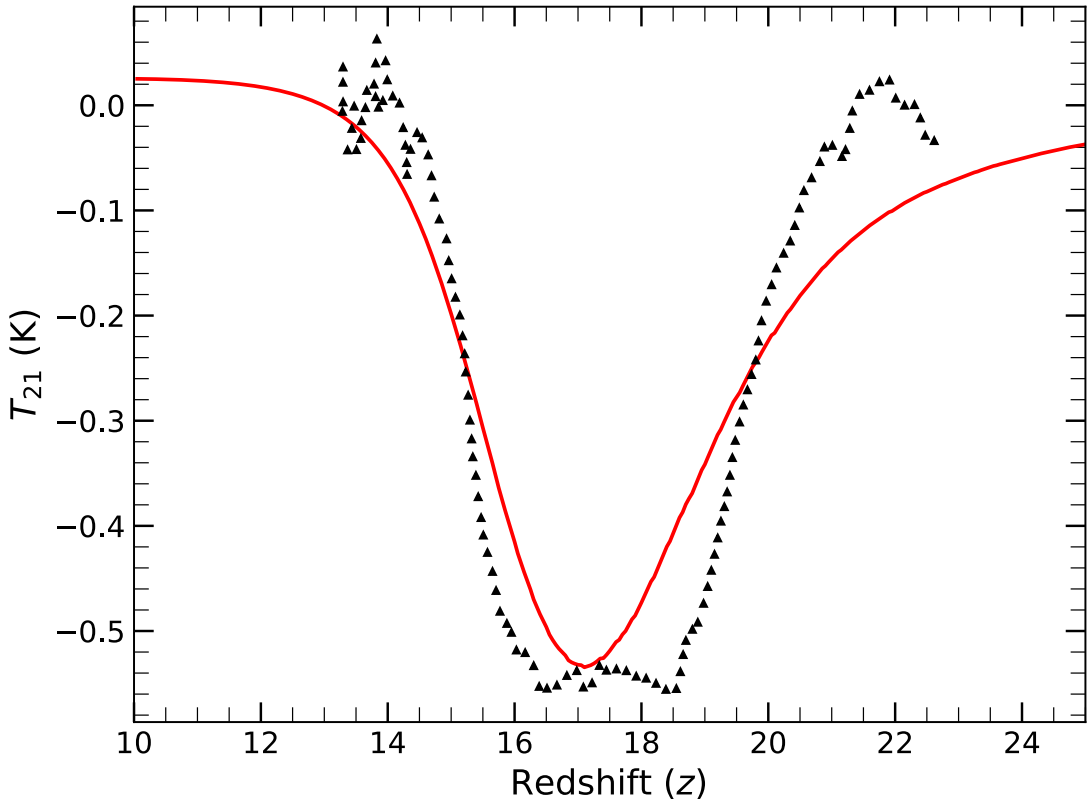

Figure 4.2: The brightness temperature, T_{21}, resulting from the temperatures shown in the bottom panel of Fig. 4.1 is represented here by red solid curve. This plot is generated considering Ly-α coupling and cosmic ray heating with efficiencies, $\epsilon_{\rm III} = 0.06$, and $\epsilon_{\rm II}$ and/or $Q_{\rm II} = 0.15$ for cosmic rays produced in Pop III and Pop II stars respectively. The dark matter-baryon interaction parameters, $(m_\chi/{\rm Gev}, \sigma_{45})$ are same as in Fig. 4.1. For reference, the measured T_{21} signal by the EDGES is shown here by black triangles.

a colder IGM resulting from dark matter-baryon interaction as adopted in our model. Thus, we will first focus our result in the light of EDGES detection. Later, we will also discuss the effect of cosmic ray heating on the global 21-cm signal in the absence of any dark matter-baryon interaction.

In the Fig. 4.2, we show the estimated global 21-cm signal using T_g and T_s as discussed in the previous sections by solid red line. For comparison, we have also plotted the measured profile of T_{21} with black triangles using publicly available data of Bowman et al. (2018a). The absorption feature starting at $z \sim 20$ arises from the coupling of T_s with T_g by Ly-α photons produced by the early generation of Pop III stars. The deeper absorption of -0.5 K is resulting from the dark matter-baryon interaction that cools the IGM temperature up to $\sim$ 1 K by $z \sim 17$. Afterward, the heating due to cosmic ray protons generated from early Pop III and Pop II stars increases the IGM temperature sharply. By $z \sim 14$, the IGM temperature exceeds the CMBR temperature due to this cosmic ray heating. This causes the sharp disappearance of the absorption feature in the 21-cm signal as detected by the EDGES collaboration. Thus we can say that the rising arm of the absorption signal matches reasonably well with the cosmic ray heating along with the dark matter-baryon interaction.

We note that, for this particular profile, a very small amount of energy gets transferred from the cosmic rays to IGM. For instance, we have used $\epsilon_{\rm III} = 0.06$, and $\epsilon_{\rm II}$ and/or $Q_{\rm II} = 0.15$ for Pop III and Pop II stars. In passing we note that, even though we focus our results in light of EDGES detection, there are controversies about the detected signal by EDGES. For example, a recent work by SARAS3 collaboration (Singh et al., 2021) has claimed a null detection of the same signal by a different experimental setup. However, cosmic ray heating is a more generic physics that one should consider while modeling the cosmic 21-cm signal. The exotic dark matter-baryon interaction was/is considered only to explain the unusually strong absorption profile detected by EDGES group. Hence, in order to highlight the effect of cosmic ray heating on 21-cm signal, and keeping in mind the controversy regarding the detected signal, we describe the effect of

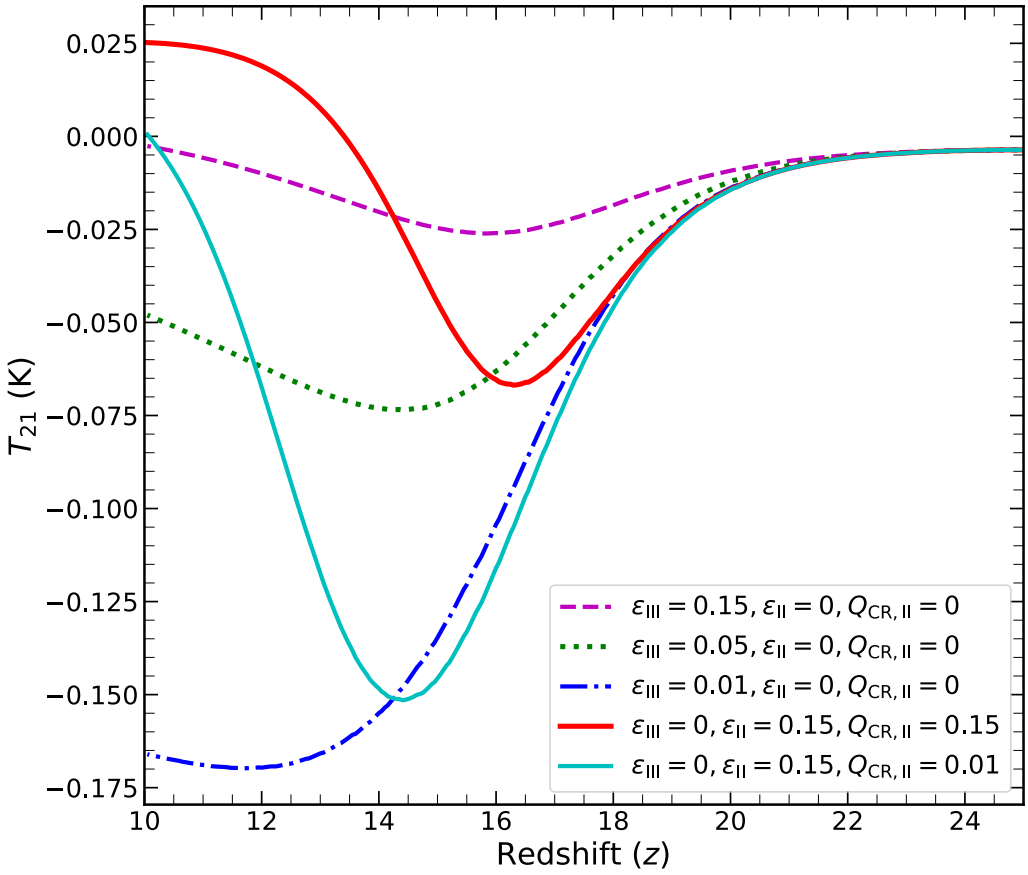

Figure 4.3: Variations in the global HI 21-cm signal T_{21} due to the various efficiencies of cosmic ray heating are shown here. We kept the spectral index of cosmic ray spectra, q fixed for this plot. All the evolutions are done here without considering any exotic mechanism such as dark matter-baryon interaction.

cosmic ray heating on 21-cm signal without considering the exotic dark matter-baryon interaction, in the next section.

4.2.4 21-cm signal without dark matter-baryon interaction

In order to understand the contribution of cosmic ray heating from Pop III and Pop II stars separately, we vary the efficiency parameters $\epsilon_{\rm III}$, $\epsilon_{\rm II}$ and the amount of energy transferring from cosmic rays to the IGM, $Q_{\rm CR,II}$ keeping the cosmic ray spectral index q fixed. The resulting brightness temperature, T_{21} as obtained for various $\epsilon_{\rm II}$, $\epsilon_{\rm III}$ and

$Q_{\rm CR,II}$ is shown in Fig. 4.3. It is clear from the figure that in all such models, the absorption profile starts at $z \sim 20$ due to the Ly-α coupling. This depends only on the star formation rates of Pop III and Pop II stars and the resulting Ly-α flux. It is independent of cosmic ray heating as long as the gas temperature remains below the CMBR temperature. However, the depth and width of the absorption spectra highly depend on the heating due to cosmic rays. For example, if the Pop III SNe are more efficient in accelerating cosmic rays i.e. $\epsilon_{\rm III} = 0.15$, we get a very shallow absorption profile of ~ -0.025 K as can be seen by magenta dashed curve in Fig. 4.3. If the efficiency is even higher, it is likely to wash out any possible 21-cm absorption profile. On the other hand, reducing the efficiency would increase the absorption depth as well as the duration of the absorption as can be seen from the green dotted and blue dash-dotted curves where $\epsilon_{\rm III} = 0.05$ & 0.01 respectively. Note that, in these three models, we didn't take any contribution of cosmic ray heating by Pop II stars. Thus we can say that a very small amount of contribution in heating by cosmic rays generated from Pop III stars ($\epsilon_{\rm III} = 0.01$), would reduce the absorption depth compared to the prediction of the same by any model where no cosmic ray heating is considered. Thus accurately determining the global 21-cm signal would constrain the contribution of cosmic ray heating which in turn can put constraints on the nature of Pop III stars during the cosmic dawn.

Finally, we show the contribution of cosmic ray heating only from Pop II stars by red solid curve in Fig. 4.3, where we assumed $\epsilon_{\rm III} = 0$, $\epsilon_{\rm II} = 0.15$ and $Q_{\rm CR,II} = 0.15$. It is clear from the figure that Pop II heating is also efficient in reducing the absorption depth as well as the duration of the absorption profile. In this case, we get a maximum absorption of -0.07 K at $z \sim 16$ which ends by $z \sim 13.5$. Even for a very small efficiency of $Q_{\rm CR,II} = 0.01$, we get an absorption depth of ~ -0.15 K as can be seen from cyan solid curve in Fig. 4.3. This also increases the duration of the absorption signal. Note that, the impact of $\epsilon_{\rm II}$ is the same as that of $Q_{\rm CR,II}$. Thus even the heating by cosmic rays generated from the Pop II stars is an important physics that one should consider while modeling the cosmic 21-cm signal. We also note that Pop III stars have a considerable impact on the global 21-cm signal at redshift $z \gtrsim 16$ in all models we consider. However, T_g, T_s,

and the resulting absorption profile depend significantly on the assumed parameters of cosmic ray heating that we discuss in the next section.

4.2.5 Variation of model parameters

In this section, we show the changes in gas temperature, spin temperature, and resulting 21-cm brightness temperature by varying our model parameters such as q, $\epsilon_{\rm III}$, and $\epsilon_{\rm II}$ that govern the energy deposition by cosmic ray particles into the IGM from both Pop III and Pop II stars. Due to the fact that the $\epsilon_{\rm II}$ and $Q_{\rm CR,II}$ alter the temperatures similarly, we are keeping $Q_{\rm CR,II}$ as same as $\epsilon_{\rm II}$. Further note that there are a few parameters of our model like IMF of Pop III stars, supernova energetic, etc that are ill-constrained and can alter our results. However, all these uncertainties affect similar ways in the final temperature history of IGM and thus variation of the efficiency parameter $\epsilon_{\rm III}$ can encompass variation in any of the above-mentioned parameters. The left panels of Fig. 4.4 show results in presence of the dark matter-baryon interaction with dark matter mass $m_\chi = 0.1$ GeV and the interaction cross-section $\sigma_{45} = 2$. The right panel shows results in the standard scenario without the dark matter-baryon interaction. In the left top, middle and bottom panels of Fig. 4.4, T_g, T_s and T_{21} are plotted respectively with the model parameters shown in the legends. We have also shown our results for the default parameters discussed above by red solid curves. Further in the top and middle panels, the black dotted curves represent the CMBR temperature. The black dashed curve in the top panel is the gas temperature where no cosmic ray heating is considered and the corresponding spin temperature is shown in the middle panel by black dashed curve for reference.

The variation w.r.t the cosmic ray spectral index q is shown by magenta lines where we consider a shallower slope of $q = 2.1$. Given the same energy input, the number of cosmic ray particles below 30 MeV decreases for a smaller q. These are the particles that take part in the collisional heating and hence the flatter slope makes the cosmic ray heating less efficient as can be seen from the figure. This further increases the absorption

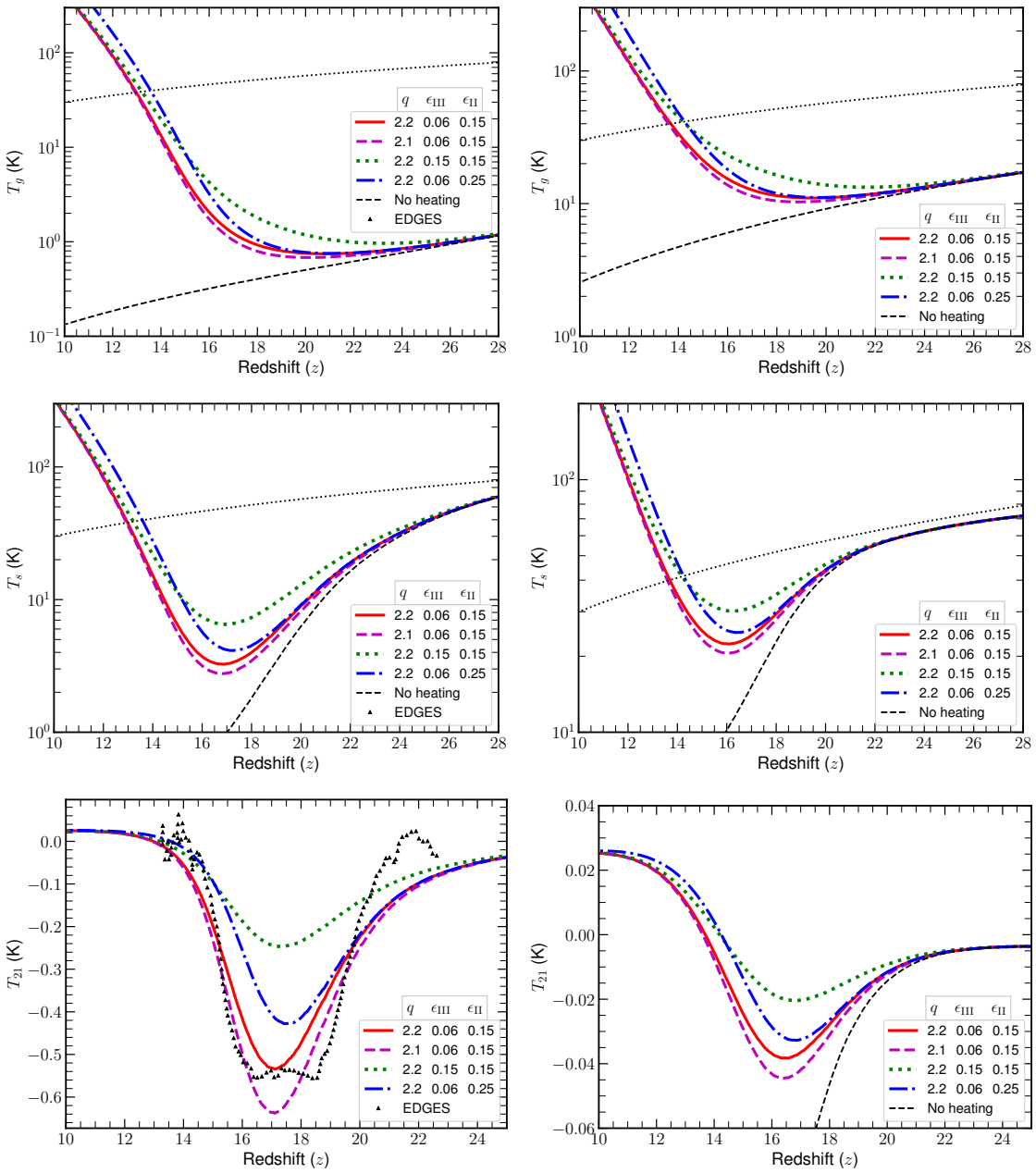

Figure 4.4: **Left panel:** The impact of cosmic ray heating on T_g, T_s and resulting T_{21} (upper to lower) are shown for different parameters describing the efficiencies of cosmic ray heating. The inset values represent the spectral index of cosmic ray spectra, q, the efficiencies of heating due to cosmic rays generated from Pop III and Pop II stars, $\epsilon_{\rm III}$ and $\epsilon_{\rm II}$ respectively. We keep the other parameter, $Q_{\rm CR,II} = \epsilon_{\rm II}$ for this figure. In this panel, the evolution of temperatures is done in the extra cooling scenario due to dark matter-baryon interaction in light of EDGES observation. The black dotted curves in the upper and middle panels represent the CMBR temperature, T_γ, whereas the black dashed curves are the temperatures where no heating source is present. **Right panel:** Same as left panel but in absence of any dark matter-baryon interaction.

depth in 21-cm signal as can be seen from bottom panel.

As already discussed in the previous sections, the cosmic ray heating is directly proportional to the efficiency parameters such as, $\epsilon_{\rm III}$ and $\epsilon_{\rm II}$. For example, it can be followed from green dotted curve that if we increase the efficiency of cosmic rays originating from Pop III stars, $\epsilon_{\rm III}$ from 6% to 15%, the dominance of Pop III stars increases significantly and the IGM temperature increases faster compared to our default model. This leads to an increase in the hydrogen spin temperature resulting in a much shallower 21-cm absorption signal of ~ -0.2 K. Similarly, if we increase the cosmic ray efficiency coming from Pop II stars, i.e from $\epsilon_{\rm II} = 15\%$ to $\epsilon_{\rm II} = 25\%$, the contribution to the heating by cosmic rays from Pop II stars increases making T_g to rise faster from $z \sim 17$. This, in turn, increases T_s which leads to a lesser depth of ~ -0.4 K T_{21} signal. It can be seen from blue dash-dotted curves in the left panel of Fig. 4.4. Thus it is clear that any higher efficiency of cosmic ray heating would be ruled out by the EDGES absorption signal. Therefore any 21-cm signal from redshift $z \sim 14 - 20$ can be used to constrain early star formation and the corresponding cosmic ray heating efficiencies.

In the right panels of Fig. 4.4, we show our results without considering any dark matter-baryon interaction that is neglecting the Eq. 2.5. All other parameters are the same as in the left panels of the figure. As expected, in general, the IGM temperature is much higher having a minimum value of ~ 10 K by $z \sim 17$ for our default parameter set (solid red curves). This resulted in a spin temperature of ~ 20 K due to the Ly-α coupling. Afterward, the IGM temperature and hence T_s increases due to the rapid cosmic ray heating. Finally, T_s crosses the CMBR temperature by $z \sim 14$ which leads to a weaker absorption profile of maximum ~ -0.04 K as can be seen from bottom right panel. The exact position of the absorption maxima depends on the interplay of Ly-α coupling and the onset of cosmic ray heating. For example, more efficient cosmic ray heating as shown by the green dotted line resulted in an absorption depth of ~ -0.02 K at an earlier redshift. Therefore, we conclude that cosmic ray heating is likely to play an important role in shaping the global 21-cm signal. In particular, it is likely to reduce

the depth of any absorption signal if at all present. In passing we note that, the Pop II stars are likely to heat the IGM by magnetosonic heating which is sensitive to the IGM magnetic field. Thus the global 21-cm signal can, in principle, be used to constrain the magnetic field during the cosmic dawn (Minoda, Tashiro, and Takahashi, 2019; Bera, Datta, and Samui, 2020).

4.2.6 Comparison with X-ray heating

There are other processes that are likely to be responsible for heating of the intergalactic medium such as, X-ray heating (Pritchard and Furlanetto, 2007; Baek et al., 2009; Ghara, Datta, and Choudhury, 2015b; Fialkov and Barkana, 2014), Ly-α (Chuzhoy and Shapiro, 2006; Ghara and Mellema, 2020; Mittal and Kulkarni, 2021), CMB (Venumadhav et al., 2018), etc. At present there is no evidence showing the domination of any heating mechanism over others. All possible heating mechanisms have their own free parameters which are not well-constrained. Thus only when more observational evidences are available, detailed modeling of 21-cm signal including all possible sources of heating is effective and that is beyond the scope of the current work. However, to demonstrate the importance of cosmic ray heating, we compare our results due to cosmic ray heating with X-ray heating without the presence of any exotic physics such as dark matter-baryon interaction. In the upper panel of Fig. 4.5, we have shown the comparison of gas (solid) and spin (dashed) temperatures for cosmic ray heating (red) and X-ray heating (blue) for the same star formation rate densities and the Ly-α coupling. In order to include the X-ray heating in our model we followed Eq. 14 given in Chatterjee, Choudhury, and Mitra (2021). In case of cosmic ray heating, we have taken the efficiencies as $\epsilon_{\rm III} = 0.1$ and $\epsilon_{\rm II}$ and/or $Q_{\rm CR,II} = 0.15$ for this particular plot. On the other hand, for X-rays the contribution to the heating from Pop III stars and Pop II stars are $f_{\rm Xh,III} = 0.001$ and $f_{\rm Xh,II} = 0.2$ which is motivated by Chatterjee, Choudhury, and Mitra (2021) and Furlanetto, Oh, and Briggs (2006a). We varied the heating rate due to X-rays coming from Pop III stars from $f_{\rm Xh,III} = 0.001$ to $f_{\rm Xh,III} = 0.1$ and the changes in temperatures are negligible as stated

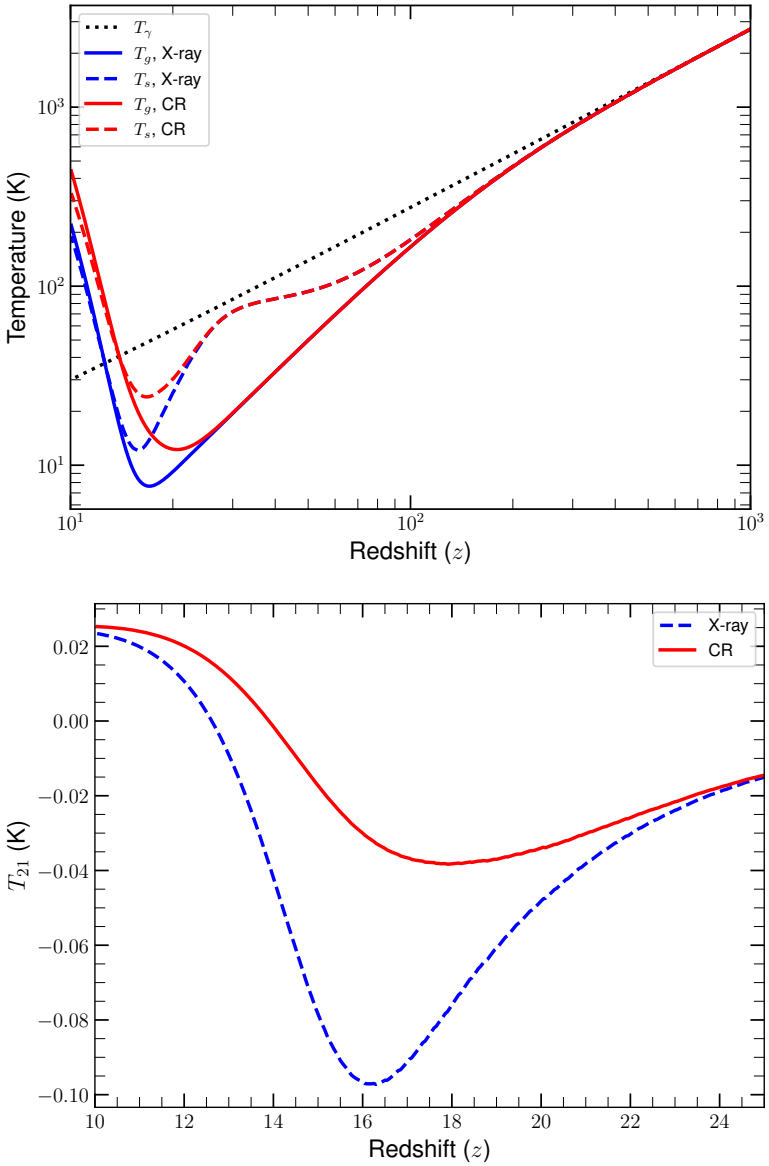

Figure 4.5: The temperature evolution shown in red is due to the presence of cosmic ray heating for the parameters $\epsilon_{\rm III} = 0.1$, $\epsilon_{\rm II}$ and/or $Q_{\rm CR,II} = 0.15$, while the temperatures shown in blue are due the X-ray heating for the parameters $f_{\rm Xh,III} = 0.001$, $f_{\rm Xh,II} = 0.2$. The resulting brightness temperatures, T_{21} are shown in the lower panel due to X-ray heating (blue dashed) and cosmic ray heating (red solid).

in Chatterjee, Choudhury, and Mitra (2021). It is clear from the blue and red curves that the contribution of cosmic rays and X-rays to the heating are quite similar. Although a small change in T_s can make a big difference in the resulting brightness temperature that is shown in the lower panel of Fig. 4.5. For the set of parameters that we used here, the cosmic ray heating is more efficient as compared to the X-ray heating for the same star formation history, though depending upon the parameters the magnitude of heating can be changed. Thus we conclude that the cosmic ray heating is comparable to X-ray heating during cosmic dawn and has similar effect to shape the global 21-cm signal.

4.3 Summary

We present a semi-analytical model of global HI 21-cm signal from cosmic dawn focusing on the heating by cosmic rays generated from the early generation of stars. In our model, we take into account both metal-free Pop III and metal-enriched Pop II stars. We consider the meta-galactic Lyman-Werner feedback on the Pop III stars along with supernova feedback in Pop II galaxies in order to calculate the star formations. The global HI 21-cm signal is calculated self-consistently taking into account the Ly-α coupling. The temperature evolution of IGM has been calculated using cosmic ray heating along with the dark matter-baryon interaction and adiabatic cooling. We consider the ionization and collisional heating by low-energy cosmic ray protons generating and escaping from Pop III halos. Besides accounting for the amount of cosmic ray energy in the IGM, our model captures the evolution of the cosmic ray spectrum, as they propagate through the IGM and lose their energy by ionizing and exciting neutral Hydrogen atoms, and due to the adiabatic expansion. We further consider the cosmic rays produced by the Pop II stars which transfer energy to the intergalactic medium through the generation of magnetosonic Alfvén waves. Here, we would like to mention that, all the quantities such as IGM kinetic/spin temperature, ionization fraction, Lyman-α/Lyman-Werner background radiation, star formation rate, etc estimated here are globally averaged quantities. In principle, one should first simulate them on 3D cubes self-consistently at differ-

ent redshifts and then perform the averaging. We must note that, although estimating the global 21-cm signal directly from the global quantities is faster, it can introduce bias in the estimated signal.

We find that the cosmic ray is an important source of IGM heating and shapes the global 21-cm signal during cosmic dawn which is in agreement with the existing literature. The depth, duration and timing of the absorption signal are highly modulated by the cosmic ray heating that we consider here. In particular, the EDGES signal can be well explained by our model of cosmic ray heating along with the Ly-α coupling and dark matter-baryon interaction with a suitable choice of efficiency parameters. In fact, the required efficiency parameters of cosmic ray heating are reasonably small like $\epsilon_{\rm III} = 0.06$ & $\epsilon_{\rm II}$ and/or $Q_{\rm CR,II} = 0.15$ to produce significant heating of the IGM and match the EDGES observed profile. Further, we explore the various efficiency parameters related to the cosmic ray heating and show that the brightness temperature highly depends on these parameters. In particular, highly efficient cosmic ray heating reduces T_{21} by a significant amount. We also showed that the cosmic rays can highly impact the IGM temperature or in turns the 21-cm signal, in absence of any dark matter-baryon interaction, and could even potentially wash out the absorption signal during cosmic dawn. Thus cosmic rays need to be considered as a potential source of IGM heating along with widely explored sources of heating such as through soft X-rays during the cosmic dawn. We further argued that, since the cosmic 21-cm signal can be highly modulated by the heating due to cosmic rays produced by the early generation of stars, accurately determined 21-cm signal by experiments such the EDGES (Experiment to Detect the Global Epoch of Reionization Signature, Bowman et al., 2018a), SARAS (Shaped Antenna measurement of the background RAdio Spectrum, Raghunathan et al., 2021), LEDA (Large-aperture Experiment to Detect the Dark Ages, Price et al., 2018), REACH (Radio Experiment for the Analysis of Cosmic Hydrogen, Lera Acedo, 2019b), SKA (Square Kilometer Arrays), HERA (Hydrogen Epoch of Reionization Array), etc. could be used to probe the early cosmic ray heating and constrain the nature of these early generations of stars.

Currently, there is only one observational evidence of global HI 21-cm signal by Bowman et al. (2018a) along with a null detection by Singh et al. (2021) during cosmic dawn. However, there are several observational constraints during the reionization and post-reionization epochs. Hence, in the following chapter, we combine the majority of the available observations from cosmic dawn and the epoch of reionization to explore the prospects of bridging the gap between these two epochs.